Particle-mediated delivery of frataxin plasmid to a human sensory neuronal model of Friedreich's Ataxia

Ewa Czuba-Wojnilowicz,[a,^] Serena Viventi,[b,^] Sara E. Howden,[c] Simon Maksour,[d] Amy Hulme,[d] Christina Cortez-Jugo,*[a] Mirella Dottori*[b,d] and Frank Caruso*[a]

[a]ARC Centre of Excellence in Convergent Bio-Nano Science and Technology, and the Department of Chemical Engineering, The University of Melbourne, Parkville, Victoria 3010, Australia. E-mail: christina.cortez@unimelb.edu.au; fcaruso@unimelb.edu.au

[b]Department of Biomedical Engineering, The University of Melbourne, Parkville, Victoria 3010, Australia. E-mail: mdottori@uow.edu.au

[c]Murdoch Children's Research Institute, and the Department of Paediatrics, The University of Melbourne, Parkville, Victoria 3010, Australia

[d]Illawarra Health and Medical Research Institute, Molecular Horizons, School of Medicine, University of Wollongong, Wollongong, NSW 2522, Australia. E-mail: mdottori@uow.edu.au

^These authors contributed equally to this work

ABSTRACT

Increasing frataxin protein levels through gene therapy is envisaged to improve therapeutic outcomes for patients with Friedreich's Ataxia (FRDA). A non-viral strategy that uses submicrometer-sized multilayered particles to deliver frataxin-encoding plasmid DNA affords up to 27000-fold increase in frataxin gene expression within 2 days *in vitro* in a stem cell-derived neuronal model of FRDA.

Friedreich ataxia (FRDA) is an autosomal recessive disease characterized by neurodegeneration and cardiomyopathy and is the most common form of all inherited ataxias known to date.[1] Prominent regions of neurodegeneration occur within the cerebellar brain region and sensory neurons of the dorsal root ganglia (DRG). FRDA occurs as a result of the presence of a trinucleotide GAA repeat expansion in the first intron of the FRATAXIN (*FXN*) gene, resulting in an insufficiency of the mitochondrial protein frataxin (FXN). Reduced levels of FXN leads to mitochondrial dysfunction, cell toxicity, and cell death.[1]

Currently used therapeutic strategies in FRDA are aimed partly at slowing down the neurodegenerative processes, but mostly on providing symptom relief. A major goal for treating FRDA is to identify therapeutic compounds that can (1) increase or sustain *FXN* expression in neuronal and cardiac cells and (2) be easily delivered to the brain and cardiac tissue. There are numerous drug therapy studies underway but results from clinical trials have been modest.[2] Alternatively, gene and cell replacement therapies have gained attention as a treatment strategy for the most severely degenerative *FXN* mutant cells. A viral strategy using adenovirus carrying a vector expressing human *FXN* was investigated on a mouse model with *FXN* deletion in cardiac and skeletal muscles.[3] This treatment fully prevented cardiomyopathy, which is the most common cause of mortality in FRDA patients and was also efficient in reversing cardiomyopathy when administered after the onset of heart failure. More recently, Piguet *et al*. reported rapid and complete reversal of the sensory ataxia by gene therapy.[4] In that study, a mouse model was used whereby *FXN* was deleted specifically in parvalbumin-expressing cells to target the proprioceptive neurons, one of the major neuronal populations responsible for the FRDA sensory ataxia. A complete rescue of the sensory neuropathy was observed using an *FXN*-expressing adenovirus delivery vector.[4] These results highlight the potential of gene therapy in FRDA-associated cardiomyopathy and neuropathy.

With the safety concerns associated with using viruses for gene delivery, there is great interest in developing non-viral approaches for the delivery of nucleic acids or other drugs, particularly to the brain.[5] Approaches include the enabling of nanotechnology to engineer inorganic, lipid, or polymer-based nanoparticles that can encapsulate proteins, DNA, and/or drugs for delivery into tissues. Their potential clinical use as drug delivery systems is rapidly growing, with nanoparticles for cancer therapy presently on the market, including the first FDA-approved nanoparticle for the delivery of small interfering RNA.[6] In FRDA, lipid nanoparticles containing *FXN* messenger RNA (mRNA) have been administered intravenously in adult mice.[7] The use of RNA transcript therapy resulted in over 50% of *mFXN* being processed to mature protein within 24 h *in vivo* and was the first reported attempt to deliver therapeutic mRNA to the DRG. However, the effect of *FXN* mRNA is short-lasting and would thus require sustained delivery to ensure continuous protein production. Hence, strategies that would ensure sustained expression of *FXN* and protein production (e.g., stable plasmid DNA integration) in neurons are desirable.

Herein, we describe the use of a versatile particle system to deliver an *FXN* expression plasmid into sensory neurons derived from FRDA-induced pluripotent stem cells (iPSC). The particles are prepared *via* the templated assembly of interacting materials in a layer-by-layer (LbL) approach to form a multilayered thin film on a spherical substrate or template.[8] Thin film formation *via* LbL assembly has been used for the preparation of polymer capsules and nanostructured coatings on planar and colloidal substrates, providing versatility in terms of substrate, composition, and interlayer interactions (e.g., electrostatic, covalent, hydrogen bonding).[9,10] Templated assembly enables precise engineering of particle properties, such as size, shape, surface chemistry, and composition.[11] The loading of drugs, including small molecular weight drugs, proteins, and nucleic acids within the template itself, embedded within the multilayer film, or adsorbed on the particle surface, has been demonstrated for various applications including cancer therapy, atherosclerosis, and vaccines.[12]

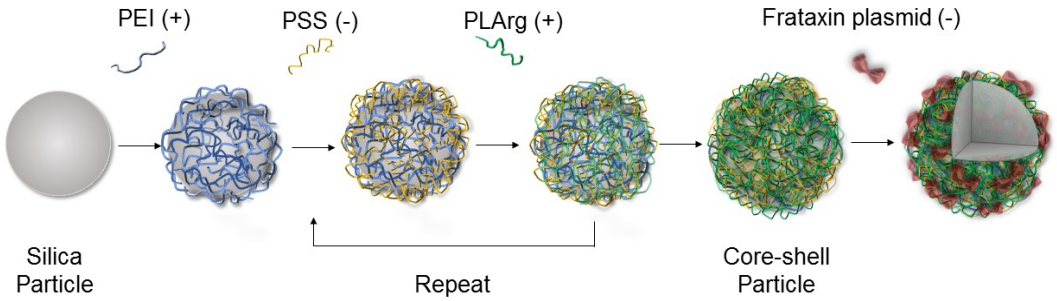

Scheme 1. Schematic illustration of LbL film assembly by deposition of alternating layers of anionic PSS and cationic PLArg polyelectrolytes on PEI-coated silica particles. PLArg-terminated particles, with a shell structure, [PEI-(PSS/PLArg)$_4$] (where n = 4 refers to 4 PSS/PLArg coating cycles), were used to bind plasmid DNA by electrostatic interactions between positively charged amine groups on PLArg and negatively charged phosphate groups on DNA.

To facilitate the loading of plasmid DNA *via* complexation on the particle surface, positively charged poly-L-arginine (PLArg)-terminated particles were prepared. Firstly, spherical silica templates were coated with a layer of polyethyleneimine (PEI) to prime multilayer growth, followed by the deposition of alternating layers of poly(sodium 4-styrenesulfonate) (PSS), as the anionic component, and PLArg as the cationic component (Scheme 1). PSS is an FDA-approved material that is used as a potassium-lowering agent in the gastrointestinal tract. PLArg is a polypeptide known to effectively bind nucleic acids, as demonstrated by the DNA binding capacity of PLArg–nucleic

acid polyplexes,[13,14] PLArg-containing films,[15,16,17] PLArg-grafted surfaces,[18,19] and PLArg-coated liposomes.[20] PLArg, as a natural polypeptide, is expected to be biocompatible. The degradability of PLArg-containing capsules by proteases has been demonstrated using LbL-assembled dextran sulfate/PLArg microcapsules,[21,22,23] which could provide a potential release mechanism for complexed DNA inside cells.

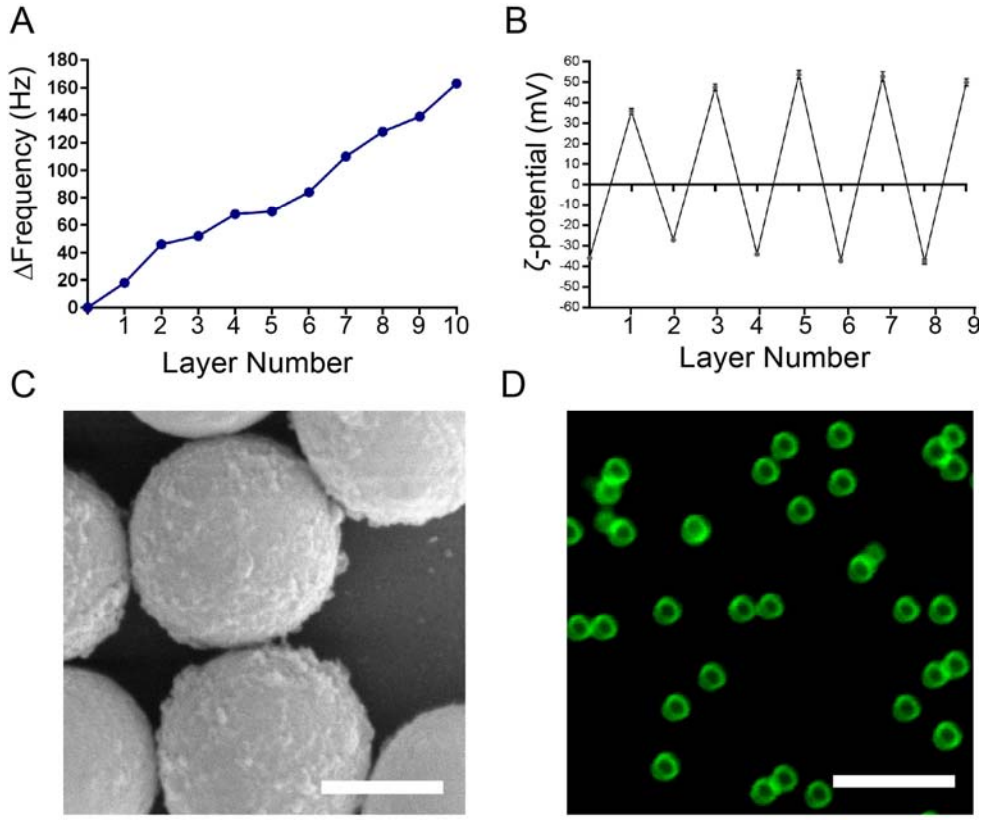

Figure 1. LbL film characterization and preparation of multilayered particles. (A) Formation of a PEI-(PSS/PLArg)$_4$ film *via* LbL as monitored by QCM-D. The odd layer numbers correspond to PLArg deposition (except Layer 1, which is PEI), and the even layer numbers correspond to PSS deposition (except Layer 10, which is DNA). (B) Corresponding microelectrophoresis data (ζ-potential) showing the LbL assembly of PSS and PLArg on the spherical silica template (Layer 0). (C) SEM image of the core–shell particles after LbL assembly. The particle core is silica and the shell structure is [PEI-(PSS/PLArg)$_4$]. Scale bar 500 nm. (D) Confocal microscopy image of fluorescently labeled particles with the shell structure [PEI-(PSS/PLArg)$_2$-(PSS/PLArg$_{AF488}$)-(PSS/PLArg)]. Scale bar 5 µm.

The LbL assembly of PSS/PLArg was monitored using quartz crystal microgravimetry with dissipation (QCM-D), as shown in Fig. 1A. QCM-D allows real-time monitoring of material deposition on a planar surface, where mass adsorbed on a surface is measured by a decrease in the resonance frequency of an oscillating piezo-electric crystal. Figure 1A shows the stepwise change in resonance frequency, reflecting the LbL adsorption of the interacting (electrostatic) polyelectrolytes. Plasmid DNA was allowed to adsorb on the PLArg-terminated [PEI-(PSS/PLArg)$_4$] film for 20 min and the observed change in resonance frequency was used to calculate the mass of deposited DNA according to Sauerbrey's equation[24]—a coverage of 0.43 μg of DNA per cm^2 was obtained. This is consistent with reported DNA complexation on polycationic surfaces, including poly-β-amino esters, where plasmid DNA coverage of up to 0.44 μg of DNA per cm^2 was observed per bilayer.[25] Atomic force microscopy (AFM) was used to confirm the presence of DNA on the film (Fig. S1). Comparison of the surface morphology/topography of PEI-(PSS/PLArg)$_2$ and PEI-(PSS/PLArg)$_2$-DNA films prepared on silicon wafers revealed an increase in film roughness of 0.8 nm after DNA adsorption, further confirming DNA binding to the PLArg-terminated surface.

The assembly process of PEI-(PSS/PLArg)$_4$ was also monitored by ζ-potential measurements after each deposition step—the pattern of charge reversal confirmed the sequential deposition of PLArg and PSS (Fig. 1B). SEM was used to assess any changes in particle diameter after LbL assembly (Fig. 1C). Measurement of 100 particles revealed a change in particle size from 951 ± 32 to 997 ± 41 nm after PEI-(PSS/PLArg)$_4$ film deposition, which corresponds to an increase of ~5 nm per layer and agrees with previous reports of similar polypeptide systems.[16] Particle monodispersity was confirmed using fluorescence microscopy (Fig. 1D), where AlexaFluor 488-labeled PLArg was used as the layer material. To improve reproducibility, reporting, and re-analysis, this study conforms to the Minimum Information Reporting in Bio–Nano Experimental Literature (MIRIBEL) standard,[26] and a companion checklist is provided in the Supplementary Information.

DNA complexation by PLArg-terminated particles was assessed using agarose gel electrophoresis. Figure 2A shows the gradual binding of 100 ng of plasmid DNA (pEGFP 3 kbp) with increasing number of particles. The complete complexation of 100 ng DNA was estimated to occur in the presence of (2–8)×10^6 particles (corresponding to an estimated surface coverage of 1961–490 ng DNA per cm^2), as indicated by the absence of free noncomplexed plasmid DNA bands on the gel. DNA adsorption is

expected to shift the particle surface charge from positive, owing to the PLArg outer layer, to negative, owing to the phosphate groups on DNA. Measurement of the ζ-potential, which is indicative of the surface charge of the particles, shows a shift from positive to negative ζ-potentials, i.e., from 54 ± 5 mV to −45 ± 4 mV. The overall negative charge on the particles is advantageous—previous reports[27] have shown that regardless of nanoparticle shape and material, negatively charged nanoparticles interact with neuronal membranes and are more efficiently internalized than positive or neutral particles.

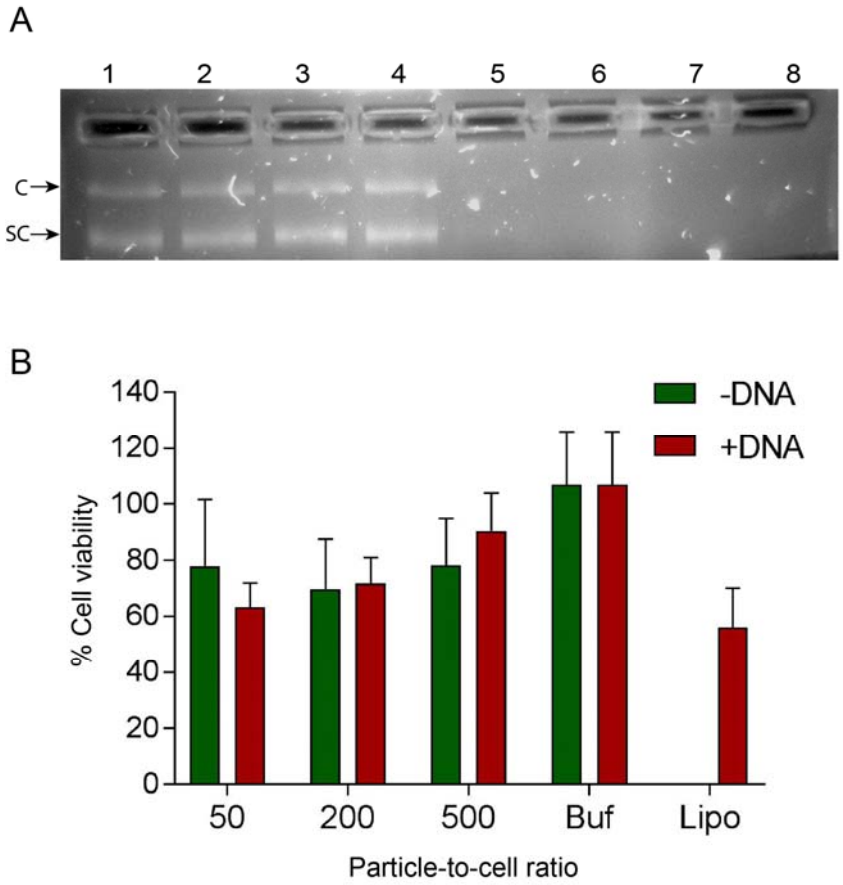

Figure 2. DNA complexation by particles and cytotoxicity in U87-MG cell line. (A) Agarose gel electrophoresis analysis of pEGFP plasmid DNA complexation by particles: Lane 1, plasmid DNA; Lanes 2–7, particle/DNA complexes at different ratios (DNA complexed by 1×10^5, 2×10^5, 2×10^6, 8×10^6, 3.6×10^7, and 7.2×10^7 particles, respectively); and Lane 8, particles only control. The two bands in Lanes 1–4 correspond to two conformations of plasmid DNA: circular (C) and supercoiled (SC). (B) Viability of cells after incubation for 24 h with bare core–shell particles (−DNA) (green) and (pcDNA3-Luc)-coated core–shell particles (+DNA) (red) added at varying particle-to-cell ratios measured by Alamar blue cell viability reagent. Controls: cells

incubated with buffer (Buf) and cells incubated with lipofectamine complexed with DNA (Lipo).

The association of DNA-coated particles was initially performed using a brain-derived glioblastoma cell line (U87-MG) as a model. Flow cytometry studies (Fig. S2A) revealed high cell association for the PLArg-terminated LbL particles (>60% of cells associated with the particles) at particle-to-cell ratios greater than 50. Particle internalization was confirmed by confocal microscopy, which showed the presence of the PLArg-terminated LbL particles inside the cells after incubation for 24 h (Fig. S2B). The cytotoxicity of the LbL particles in the U87-MG cells was also investigated. Cells were incubated at increasing particle-to-cell ratios, using PLArg-terminated particles and particles pre-incubated with DNA (0.5 μg DNA). Here, plasmid DNA encoding luciferase (pcDNA3-Luc; 5.9 kbp) was used instead of pEGFP to avoid potential fluorescence interference with the Alamar blue cell viability assay. Using the assay, at least 70% cell viability was observed at particle-to-cell ratios above 50 (Fig. 2B). Importantly, under these conditions (24 h incubation), DNA delivery using the presently engineered particles attained a higher cell viability than the commonly used transfection reagent lipofectamine. It is worth noting that while pEGFP (3 kbp) and pcDNA3-Luc (5.9 kbp) were used to determine the complexation efficiency and toxicity of the DNA-coated particles, respectively, plasmid size is expected to have little influence on the viability of the cells if the same mass of DNA (0.5 μg) is used for particle complexation. Irrespective of plasmid size, the same mass of plasmid DNA will have the same number of bases and phosphate groups, and hence is likely to impart similar surface composition and net charge on the particles.

Given the low cytotoxicity and high cell association of the particles with U87-MG cells, we examined the uptake of the PLArg-terminated LbL particles by sensory neurons generated from patient derived-FRDA iPSCs. FRDA iPSC cells were differentiated to sensory neurons using our previously published protocols.[28,29] Characterization of the differentiated sensory neurons was performed by immunostaining using peripherin as a specific marker for peripheral neurons and markers associated with the three major subpopulations of DRG sensory neurons: nociceptors (tropomyosin receptor kinases A or TRKA); mechanoreceptors (tropomyosin receptor kinases B or TRKB); and proprioceptors (tropomyosin receptor kinases C or TRKC, osteopontin and

parvalbumin) (Fig. S3). The binding and uptake of fluorescently labeled PLArg-terminated particles with complexed model plasmid DNA (pcDNA3-Luc) in neurons was assessed following incubation of the particles for 24 h. The presence of labeled particles was confirmed within the cytoplasm of FRDA iPSC-derived sensory neurons, suggesting their efficient uptake (Fig. 3A).

These experiments were repeated using an *FXN*-green fluorescent protein (GFP) expression plasmid (8.9 kbp). FRDA iPSC-derived sensory neurons were treated with either bare LbL particles or LbL particles coated with *FXN* expression plasmid for 24 h, after which the cells were washed and cultured for another 24 h or 13 days. Cells were washed three times prior to quantitative polymerase chain reaction (Q-PCR) analyses to remove excess plasmid and/or particles. Q-PCR analyses were performed to examine *FXN* cDNA levels in each treatment group. *FXN* levels were compared to the endogenous *FXN* levels found in the control sample group, i.e., untreated sensory neurons (Cells). The relative increase in *FXN* levels compared to the control group is presented as fold change in Fig. 3C. The data showed approximately 27000-fold increase in *FXN* levels in cells treated for 2 days with particles with bound *FXN*-GFP expression plasmid relative to the control treatment samples. Relatively high *FXN* levels (1300-fold increase) were also observed at 14 days following particle treatment, however the upregulation of FXN expression at the protein level remains to be demonstrated by western blot or similar protein detection techniques. The high induction of *FXN* levels in the sensory neurons is likely due to PLArg. Arginine-rich peptides have been found to enhance the intracellular translocation of various cargos via membrane-penetrating properties.[30] In addition, nuclear localization signals (NLS) that transport proteins to the cell nucleus are often arginine-rich, [31] which may provide an additional benefit for the use of PLArg to enhance nuclear entry and transfection.

It has previously been shown that exceedingly high levels of FXN in human cells can cause toxicity and oxidative stress.[32] Hence, the expression of the cell death marker, Caspase 3 *(CASP3)*, was examined in all treatment groups to determine whether particle treatment was toxic to the sensory neurons. The Alamar blue cell viability assay was not suitable for testing the viability of FRDA sensory neurons because they are non-dividing cells; hence, the viability of the treated neurons was tested by measuring *CASP3* expression using Q-PCR. No significant difference in *CASP3* cDNA expression

was observed across all treatment groups at both Day 2 and Day 14 after treatment (Fig. 3D), which suggests the high biocompatibility of the particles in neurons *in vitro* and the tolerance of the cells to high levels of *FXN* expression.

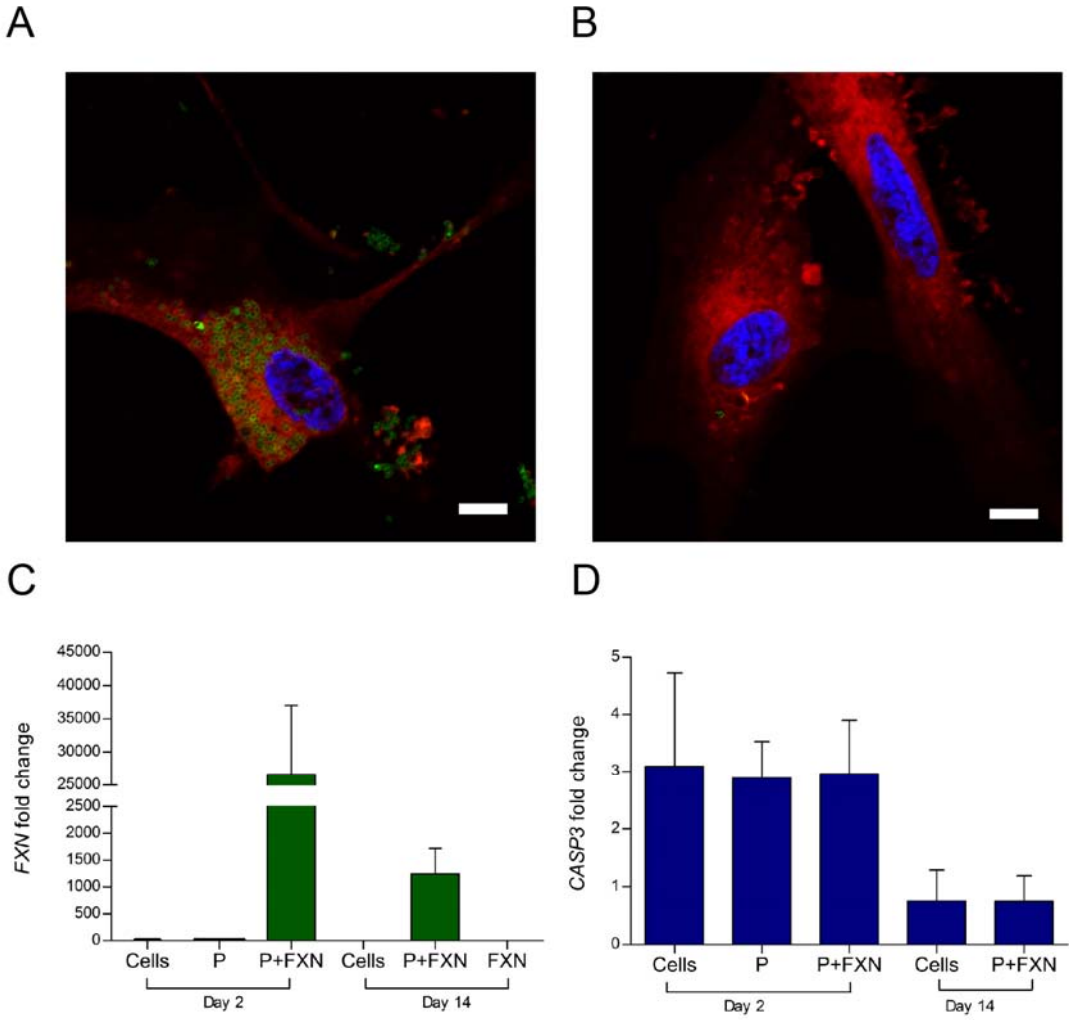

Figure 3. Particle internalization and Q-PCR analyses for assessing expression of *FXN* and *CASP3* in FRDA iPSC-derived sensory neurons. Confocal microscopy images of (A) cells treated with LbL particles (green) coated with pcDNA3-Luc plasmid DNA and (B) untreated cells. Plasma membranes were stained with CellMask reagent (red). Nuclei were stained with Hoechst 33342 (blue). Scale bars 10 μm. Fold change of (C) *FXN* cDNA levels ($2^{(-\Delta\Delta CT)}$ analysis method, $n = 3$) and (D) *CASP3* cDNA levels ($2^{(-\Delta\Delta CT)}$ analysis method, $n = 3$) in FRDA iPSC-derived sensory neurons following 2 or 14 days treatment with either bare LbL particles (P) or LbL particles coated with *FXN* expression plasmid (P+FXN) relative to non-treated neurons (Cells). Data are shown as the average mean ± standard error of the mean, with $n = 3$ biological

replicate experiments and $n > 3$ technical replicate samples for each replicate experiment.

In summary, highly biocompatible PLArg-containing LbL particles were engineered and examined for the effective delivery of *FXN* expression plasmid in FRDA iPSC-derived sensory neurons. Up to a 27000-fold increase in *FXN* expression was observed following treatment for 2 days, when compared to the untreated control samples. In addition, the study demonstrates that FRDA iPSC-derived sensory neurons represent a suitable platform for screening various nanoparticle types for uptake by neurons and delivery of DNA and/or drugs to treat FRDA. The present findings highlight the potential of the templated LbL particles for therapeutic use as delivery systems to neurons as well as the importance of a versatile system to allow further engineering to navigate the biological barriers for effective brain delivery or potentially target of specific neuronal types.[33] In FRDA disease, one of the three subpopulations of sensory neurons, proprioceptive neurons or proprioceptors, are predominantly affected,[34] and a more precise therapy could be proposed through functionalization of nanoparticles *via* antibodies to target this neuronal population. Nanoparticles could therefore facilitate the ultimate goal of plasmid delivery to treat FRDA, which is for the plasmid DNA to be effectively delivered to the nucleus of target cells and to produce frataxin at non-toxic levels.

Acknowledgements

This research was conducted and funded by the Australian Research Council Centre of Excellence in Convergent Bio-Nano Science and Technology (project number CE140100036). F.C. acknowledges the award of a National Health and Medical Research Council Senior Principal Research Fellowship (GNT1135806). S.V. was funded by a Melbourne International Research Scholarship and a Melbourne International Fee Remission Scholarship (The University of Melbourne). This work was performed in part at the Materials Characterisation and Fabrication Platform (MCFP) at The University of Melbourne and the Victorian Node of the Australian National Fabrication Facility (ANFF). This study was also supported by funding from the National Ataxia Foundation, Friedreich's Ataxia Research Alliance USA, Friedreich's Ataxia Research Association Australasia, The University of Melbourne and University of Wollongong. We thank Dr. Gyeongwon Yun and Zhixing Lin for their assistance with AFM and SEM imaging, respectively. All experiments were

performed in accordance with the Guidelines of the National Health and Medical Research Council, and experiments were approved by the ethics committee at The University of Melbourne (#1545394 and #0829937). Informed consents were obtained from human participants of this study.

References

1. M. V. Evans-Galea, A. Pebay, M. Dottori, L. A. Corben, S. H. Ong, P. J. Lockhart and M. B. Delatycki, *Hum. Gene Ther.*, 2014, **25**, 684–693.
2. Y. Li, U. Polak, A. D. Bhalla, N. Rozwadowska, J. S. Butler, D. R. Lynch, S. Y. R. Dent and M. Napierala, *Mol. Ther.*, 2015, **23**, 1055–1065.
3. M. Perdomini, B. Belbellaa, L. Monassier, L. Reutenauer, N. Messaddeq, N. Cartier, R. G. Crystal, P. Aubourg and H. Puccio, *Nat. Med.*, 2014, **20**, 542–547.
4. F. Piguet, C. de Montigny, N. Vaucamps, L. Reutenauer, A. Eisenmann and H. Puccio, *Mol. Ther.*, 2018, **26**, 1940–1952.
5. S. J. Gray, K. T. Woodard and R. J. Samulski, *Ther. Delivery*, 2010, **1**, 517–534.
6. D. Adams, A. Gonzalez-Duarte, W. D. O'Riordan, C. C. Yang, M. Ueda, A. V. Kristen, I. Tournev, H. H. Schmidt, T. Coelho, J. L. Berk, K. P. Lin, G. Vita, S. Attarian, V. Plante-Bordeneuve, M. M. Mezei, J. M. Campistol, J. Buades, T. H. Brannagan, B. J. Kim, J. Oh, Y. Parman, Y. Sekijima, P. N. Hawkins, S. D. Solomon, M. Polydefkis, P. J. Dyck, P. J. Gandhi, S. Goyal, J. Chen, A. L. Strahs, S. V. Nochur, M. T. Sweetser, P. P. Garg, A. K. Vaishnaw, J. A. Gollob and O. B. Suhr, *N. Engl. J. Med.*, 2018, **379**, 11–21.
7. J. F. Nabhan, K. M. Wood, V. P. Rao, J. Morin, S. Bhamidipaty, T. P. LaBranche, R. L. Gooch, F. Bozal, C. E. Bulawa and B. C. Guild, *Sci. Rep.*, 2016, **6**, 20019.
8. F. Caruso, R. A. Caruso and H. Mohwald, *Science*, 1998, **5391**, 1111–1114.
9. J. J. Richardson, M. Bjornmalm and F. Caruso, *Science*, 2015, **348**, 2491–11.
10. J. F. Quinn, A. P. R. Johnston, G. K. Such, A. N. Zelikin and F. Caruso, *Chem. Soc. Rev.*, 2007, **35**, 707–718.
11. M. Bjornmalm, J. Cui, N. Bertleff-Zieschang, D. Song, M. Faria, M. A. Rahim and F. Caruso, *Chem. Mater.*, 2017, **29**, 289–306.
12. J. Cui, J. J. Richardson, M. Bjornmalm, M. Faria and F. Caruso, *Acc. Chem. Res.*, 2016, **49**, 1139–1148.
13. N. Emi, S. Kidoaki, K. Yoshikawa and H. Saito, *Biochem. Biophys. Res. Commun.*, 1997, **231**, 412–424.
14. A. Mann, G. Thakur, V. Shukla, A. K. Singh, R. Khanduri, R. Naik, Y. Jiang, N. Kalra, B. S. Dwarakanath, U. Langel and M. Ganguli, *Mol. Pharm.*, 2011, **8**, 1729–1741.
15. G. B. Sukhorukov, H. Mohwald, G. Decher and Y. M. Lvov, *Thin Solid Films*, 1996, **284**, 220–223.
16. L. Szyk-Warszynska, K. Kilan and R. P. Socha, *J. Colloid Interface Sci.*, 2014, **423**, 76–84.
17. J. L. Webber, N. L. Benbow, M. Krasowska and D. A. Beattie, *Colloids Surf. B*, 2017, **159**, 468–476.

18. M. Kar, N. Tiwari, M. Tiwari, M. Lahiri and S. S. Gupta, *Part. Part. Syst. Charact.*, 2013, **30**, 166–179.
19. R. J. Mudakavi, S. Vanamali, D. Chakravortty and A. M. Raichur, *RSC Advances*, 2017, **7**, 7022–7032.
20. P. Opanasopit, J. Tragulpakseerojn, A. Apirakaramwong, T. Ngawhirunpat, T. Rojanarata and U. Ruktanonchai, *Int. J. Nanomed.*, 2011, **6**, 2245–2252.
21. B. G. De Geest, R. E. Vandenbroucke, A. M. Guenther, G. B. Sukhorukov, W. E. Hennink, N. N. Sanders, J. Demeester and S. C. De Smedt, *Adv. Mater.*, 2006, **18**, 1005–1009.
22. P. R. Gil, S. De Koker, B. G. De Geest and W. J. Parak, *Nano Lett.*, 2009, **9**, 4398–4402.
23. S. De Koker, B. G. De Geest, C. Cuvelier, L. Ferdinande, W. Deckers, W. E. Hennink, S. C. De Smedt and N. Mertens, *Adv. Funct. Mater.*, 2007, **17**, 3754–3763.
24. G. Sauerbrey, *Z. Phys.*, 1959, **155**, 206.
25. R. J. Fields, C. J. Cheng, E. Quijano, C. Weller, N. Kristofik, N. Duong, C. Hoimes, M. E. Egan and W. M. Saltzman, *J. Controlled Release*, 2012, **164**, 41–48.
26. M. Faria, M. Bjornmalm, K. J. Thurecht, S. J. Kent, R. G. Parton, M. Kavallaris, A. P. R. Johnston, J. J. Gooding, S. R. Corrie, B. J. Boyd., P. Thordarson, A. K. Whittaker, M. M. Stevens, C. A. Prestidge, C. J. H. Porter, W. J. Parak, T. P. David, E. J. Crampin and F. Caruso, *Nat. Nanotechnol.*, 2018, **13**, 777–785.
27. S. Dante, A. Petrelli, E. M. Petrini, R. Marotta, A. Maccione, A. Alabastri, A. Quarta, F. De Donato, T. Ravasenga, A. Sathya, R. Cingolani, R. Proietti Zaccaria, L. Berdondini, A. Barberis and T. Pellegrino, *ACS Nano*, 2017, **11**, 6630–6640.
28. K. D. Abu-Bonsrah, S. Viventi, D. Newgreen and M. Dottori, in *Neural Crest Cells: Methods and Protocols*, eds. Q. Schwarz and S. Wiszniak, Humana Press, New York, 2019, Volume 1976, Chapter 3, 37–47.
29. A. Alshawaf, S. Viventi, W. Qiu, G. D'Abaco, B, Nayagam, M. Erlichster, G. Chana, I. Everall, J. Ivanusic, S. Skafidas and M. Dottori, *Sci. Rep.*, 2018, **8,** 603.
30. A. El-Sayed, S. Futaki and H. Harashima, *AAPS J.*, 2009, **11**, 13–22.
31. R. Cartier and R. Reszka, *Gene Ther.*, 2002, **9**, 157–167.
32. T. Vannocci, R. N. Manzano, O. Beccalli, B. Bettegazzi, F. Grohovaz, G. Cinque, A. de Riso, L. Quaroni, F. Codazzi and A. Pastore, *Dis. Models Mech.*, 2018, **11**, dmm032706.
33. D. Furtado, M. Bjornmalm, S. Ayton, A. I. Bush, K. Kempe, and F. Caruso, *Adv. Mater.*, 2018, **30**, 1801362.
34. B. Marty, G. Naeije, M. Bourguignon, V. Wens, V. Jousmäki, D. R. Lynch, W. Gaetz, S. Goldman, R. Hari, M. Pandolfo and X. De Tiège, *Neurology*, 2019, **93**, 116–124.

Table of contents entry

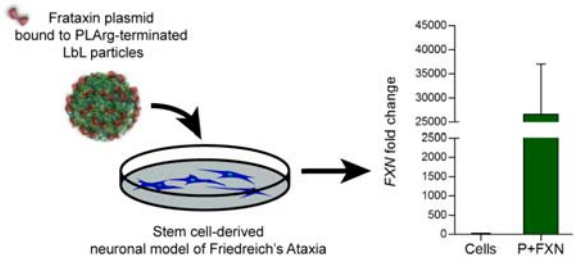

Multilayered particles in gene therapy for Friedreich's ataxia induce a 27000-fold increase in frataxin gene expression in patient-derived cell model.

Author/s:
Czuba-Wojnilowicz, E; Viventi, S; Howden, SE; Maksour, S; Hulme, AE; Cortez-Jugo, C; Dottori, M; Caruso, F

Title:
Particle-mediated delivery of frataxin plasmid to a human sensory neuronal model of Friedreich's ataxia.

Date:
2020-05-07

Citation:
Czuba-Wojnilowicz, E., Viventi, S., Howden, S. E., Maksour, S., Hulme, A. E., Cortez-Jugo, C., Dottori, M. & Caruso, F. (2020). Particle-mediated delivery of frataxin plasmid to a human sensory neuronal model of Friedreich's ataxia.. Biomaterials Science, 8 (9), https://doi.org/10.1039/c9bm01757g.